The Astronomical Journal, 165:190 (9pp), 2023 May https://doi.org/10.3847/1538-3881/acc461

Zwicky Transient Facility and Globular Clusters: The Period–Luminosity and Period–Wesenheit Relations for SX Phoenicis Variables in the *gri* Band

Chow-Choong Ngeow[1], Anupam Bhardwaj[2], Matthew J. Graham[3], Brian F. Healy[4], Russ R. Laher[5], Reed Riddle[6], and Avery Wold[5]
[1] Graduate Institute of Astronomy, National Central University, 300 Jhongda Road, 32001 Jhongli, Taiwan; cngeow@astro.ncu.edu.tw
[2] INAF-Osservatorio astronomico di Capodimonte, Via Moiariello 16, I-80131 Napoli, Italy
[3] Division of Physics, Mathematics, and Astronomy, California Institute of Technology, Pasadena, CA 91125, USA
[4] School of Physics and Astronomy, University of Minnesota, Minneapolis, MN 55455, USA
[5] IPAC, California Institute of Technology, 1200 E. California Boulevard, Pasadena, CA 91125, USA
[6] Caltech Optical Observatories, California Institute of Technology, Pasadena, CA 91125, USA
Received 2023 February 1; revised 2023 March 1; accepted 2023 March 13; published 2023 April 4

Abstract

SX Phoenicis (SXP) variables are short-period pulsating stars that exhibit a period–luminosity (PL) relation. We derived the *gri*-band PL and extinction-free period–Wesenheit (PW) relations, as well as the period-color and reddening-free period-Q-index relations for 47 SXP stars located in 21 globular clusters, using the optical light curves taken from Zwicky Transient Facility. These empirical relations were derived for the first time in the *gri* filters except for the *g*-band PL relation. We used our *gi*-band PL and PW relations to derive a distance modulus to Crater II dwarf spheroidal which hosts one SXP variable. Assuming that the fundamental and first-overtone pulsation mode for the SXP variable in Crater II, we found distance moduli of 20.03 ± 0.23 mag and 20.37 ± 0.24 mag, respectively, using the PW relation, where the latter is in excellent agreement with independent RR Lyrae based distance to Crater II dwarf galaxy.

Unified Astronomy Thesaurus concepts: SX Phoenicis variable stars (1673); Distance indicators (394); Wide-field telescopes (1800); Sky surveys (1464); Globular star clusters (656)

1. Introduction

SX Phoenicis (hereafter SXP; see, for examples, Nemec & Mateo 1990; McNamara 1997) variable stars represent a class of low-metallicity and Population II pulsating stars with periods in the range of ∼0.01 to ∼0.1 days. These pulsating stars are located in the lower main sequence on the Hertzsprung–Russell (H-R) diagram, similar to Population I δ Scuti stars—the counterparts of SXP stars with higher metallicity (near Solar). Sometimes, SXP and δ Scuti stars are collectively known as dwarf Cepheids. In globular clusters, SXP stars can also occupy the blue stragglers region on the H-R diagram.

Despite being intrinsically fainter than classical pulsating stars such as Cepheids and RR Lyrae, SXP stars are distance indicators and have been used to derive distance to stellar systems in the past (McNamara 2011), including Carina dwarf galaxy (McNamara 1995; Vivas & Mateo 2013) and a number of globular clusters (for several recent examples, see Figuera Jaimes et al. 2013; Kunder et al. 2013; Arellano Ferro et al. 2015; Deras et al. 2019; Ahumada et al. 2021). This is because SXP stars also obey a period–luminosity (PL) relations similar to other classical pulsating stars. Examples of the empirical PL, or the period–luminosity–metallicity, relations for SXP stars can be found in Nemec & Mateo (1990), Nemec et al. (1994), McNamara (1995), Pych et al. (2001), Jeon et al. (2003), Jeon et al. (2004), Cohen & Sarajedini (2012), Fiorentino et al. (2014), Kopacki (2015), Martinazzi et al. (2015a), Martinazzi et al. (2015b), and Lee et al. (2016). Some derivations of the PL relations included both SXP and δ Scuti stars (Poretti et al. 2008; McNamara 2011; Barac et al. 2022), at which two recent works suggested the PL relation for δ Scuti stars could be broken (Gaia Collaboration et al. 2022) or segmented (Martínez-Vázquez et al. 2022). In terms of theoretical studies, Santolamazza et al. (2001), Templeton et al. (2002), and Fiorentino et al. (2015) presented theoretical PL relations for SXP (and δ Scuti) stars. Since SXP stars can pulsate in radial modes (fundamental, first-overtone, and second-overtone) and/or in nonradial modes, their PL(Z) relations were primarily derived for the fundamental-mode SXP stars (in some cases the first-overtone mode SXP stars were also included).

The empirical PL(Z) relations presented in the previous work were mainly in the optical *B* and/or *V* band, with a few exceptions such as Arellano Ferro et al. (2011; including *I* band) and Vivas et al. (2019; including *g* band). Beyond optical bands, Navarrete et al. (2017) derived the near-infrared JK_s-band PL relations based on the fundamental-mode SXP stars found in ω Centauri. Nowadays, subsets of the Sloan Digital Sky Survey (SDSS) *ugriz* filters or their variants are widely used in a variety of synoptic sky surveys. For example, Vivas et al. (2020) discovered one SXP star in the Crater II dwarf galaxy using *gi*-band time-series observations taken with the Dark Energy Camera (DECam; Flaugher et al. 2015). In the coming years, the Vera C. Rubin Observatory Legacy Survey of Space and Time (LSST; Ivezić et al. 2019) will conduct a 10 yr synoptic survey in the *ugrizy* filters. The LSST is expected to discover new dwarf galaxies and identify new SXP stars in nearby dwarf galaxies. Therefore, it is useful to derive PL relations for SXP stars in the available Sloan-like filters for their application as a distance indicators in the LSST era.

The Zwicky Transient Facility (ZTF; Bellm & Kulkarni 2017; Bellm et al. 2019; Graham et al. 2019) is a synoptic imaging survey on the northern sky. The ZTF observing system

consists of a 600 megapixel mosaic CCD camera and the 48 inch Samuel Oschin Telescope in Schmidt design, providing a field-of-view of 47 square degree with a pixel scale of $1\farcs01$ pixel^{-1} (Dekany et al. 2020). Time-series observations of ZTF were conducted in the customized *gri* filters, and calibrated to PAN-STARRS1 (Chambers et al. 2016; Magnier et al. 2020) AB magnitude system (Masci et al. 2019). Therefore, the main goal of our work is to derive the *gri*-band PL relations for SXP stars located in the northern globular clusters using ZTF light curves.

The structure of this paper is organized as follow. Section 2 describes the sample of SXP stars and their ZTF light curves data. In Section 3, we refined the periods for these SXP stars and obtained their mean magnitudes based on the fitted ZTF light curves. After identifying the pulsation modes for the final selected sample of SXP stars, we derived the PL and the extinction-free period–Wesenheit (PW) relations for SXP stars in Section 4. We tested our PL and PW relations using one SXP star in Crater II dwarf galaxy by determining its distance in Section 5. The conclusions of our work are presented in Section 6.

2. Sample and Data

Early compilations of SXP stars in globular clusters were presented in Rodríguez & López-González (2000) and Santolamazza et al. (2001), and subsequently updated by Cohen & Sarajedini (2012) with a list of 263 SXP stars. Besides the Cohen & Sarajedini (2012) catalog, the "Updated Catalog of Variable Stars in Globular Clusters" (Clement et al. 2001; Clement 2017; hereafter Clement's Catalog) has also compiled a list of SXP stars in the globular clusters. After excluding those SXP stars located south of decl. -30° (as they are outside the visibility of ZTF), there are 111 and 128 SXP stars left in the Cohen & Sarajedini (2012) catalog and the Clement's Catalog, respectively, with 94 common SXP stars between these two catalogs.

We merged the SXP stars in these two catalogs, together with newly identified SXP stars in various globular clusters from recent work. These include NGC 288 (Martinazzi et al. 2015a, 2015b; Lee et al. 2016), NGC 1904/M79 (Kopacki 2015), NGC 4147 (Lata et al. 2019), NGC 5053 (Arellano Ferro et al. 2010), NGC 6205/M13 (Deras et al. 2019), NGC 6218/M12 (Kaluzny et al. 2015), NGC 6254/M10 (Salinas et al. 2016; Rozyczka et al. 2018; Arellano Ferro et al. 2020), NGC 6341/M92 (Yepez et al. 2020), NGC 6402/M14 (Yepez et al. 2022), NGC 6656/M22 (Rozyczka et al. 2017), NGC 6779/M56 (Deras et al. 2022), NGC 6934 (Yepez et al. 2018), and NGC 7089/M2 (Salinas et al. 2016).

Furthermore, we rejected SXP stars with uncertain classification or membership, as well as those not a member of the globular clusters. The rejected SXP stars are: V83 in NGC 2419 (Clement 2017), SX8, SX17, and SX24 in NGC 5024 (Bramich et al. 2012), BS19 in NGC 5053 (Arellano Ferro et al. 2010), V25 in NGC 6093 (Clement 2017), V24 in NGC 6218 (Sariya et al. 2018), V8, V9, V11, and V14 in NGC 6254 (Rozyczka et al. 2018; Arellano Ferro et al. 2020), V34 and V36 in NGC 6341 (Yepez et al. 2020), V6 in NGC 6366 (Sariya & Yadav 2015), KT-05 in NGC 6656 (Rozyczka et al. 2017), V11 in NGC 6779 (Clement 2017), and QU Sge in NGC 6838/M71 (McCormac et al. 2014).[7] Four SXP stars in NGC 5272 (Anon, SE174, NW449, and NW858) were also removed from the sample because no accurate celestial coordinates can be found for them.

All together, our sample contains 161 SXP stars located in 29 globular clusters. ZTF light curves for these SXP stars were extracted from the PSF (point-spread function) catalogs, produced from the dedicated ZTF reduction pipeline (Masci et al. 2019), using a search radius of $1''$. These PSF catalogs include those from the ZTF Public Data Release 13 and ZTF partner surveys[8] until 2022 September 30. Out of the 161 SXP stars in our sample, 19 of them do not have ZTF data, and 21 of them have very sparse ZTF light curve data (with total number of data points less than 20 in all *gri* bands). These 40 SXP stars were excluded for further analysis.

3. Periods Refinement and Light Curve Fitting

3.1. Two-step Period Refining Process

Similar to our previous work (Ngeow et al. 2022b), we refined the pulsation periods for the 121 SXP stars, selected in previous section with sufficient number of observations, using the `LombScargleMultiband` (LSM) module (VanderPlas & Ivezić 2015)[9] in a two-step process. The first step is running the LSM module on the *gri*-band (whenever available) ZTF light curves for each SXP stars within a period range of 0.005–0.500 days. We then fold the light curves based on the determined periods, and fit the folded light curves using a low-order Fourier expansion (for example, see Deb & Singh 2009; Bhardwaj et al. 2015; Ngeow et al. 2022b). Data points deviated more than 3 s, where s is the dispersion of the fitted light curve, were discarded and the LSM module was run for the second time to determine the final adopted periods ($P_{\rm LSM}$).

3.2. LOWESS-assisted Fourier Fitting

In our previous work, we selected the best n-order of the Fourier expansion via visual inspection. Alternatively, the best Fourier order can be determined using the Baart's condition (Petersen 1986; Deb & Singh 2009). However, based on our past experience, the Baart's condition might not always work. An example is shown in Figure 1, at which Baart's condition suggested the best Fourier order is $n = 6$ for this light curve. Clearly, the fitted sixth-order Fourier expansion resulted some of the small numerical bumps seen around phases of $\sim$0.5 to $\sim$0.8.

Since the shapes of the light curves for pulsating stars are either sawtooth-like or sinusoidal, the best-fit Fourier expansion should be close to a smoothed light curve portraited by the observed data points. We employed the nonparametric LOcally WEighted Scatterplot Smoothing (LOWESS; Cleveland 1979) algorithm, implemented in `statsmodels` package, to smooth the observed light curve. Nevertheless, such a smoothed curve will not be continuous crossing phase 0 or 1 (i.e., nonperiodic), and might not fit well the data points at the "borders" (i.e., at phases close to 0 or 1) of the light curve. To remedy these problems, we duplicated the observed light curves such that the observed light curve spanned from phase 0 to 2 (hence, forcing the continuity at phase 1), and applied LOWESS algorithm to

[7] QU Sge is a semidetached binary system, where its primary is a SXP star (Jeon et al. 2006), which could be a foreground star (McCormac et al. 2014).

[8] The high-level ZTF surveys are divided into public surveys, partner surveys and California Institute of Technology (Caltech) surveys, see Bellm et al. (2019) for more details.

[9] Available in the `astroML/gatspy` package from https://github.com/astroML/gatspy.

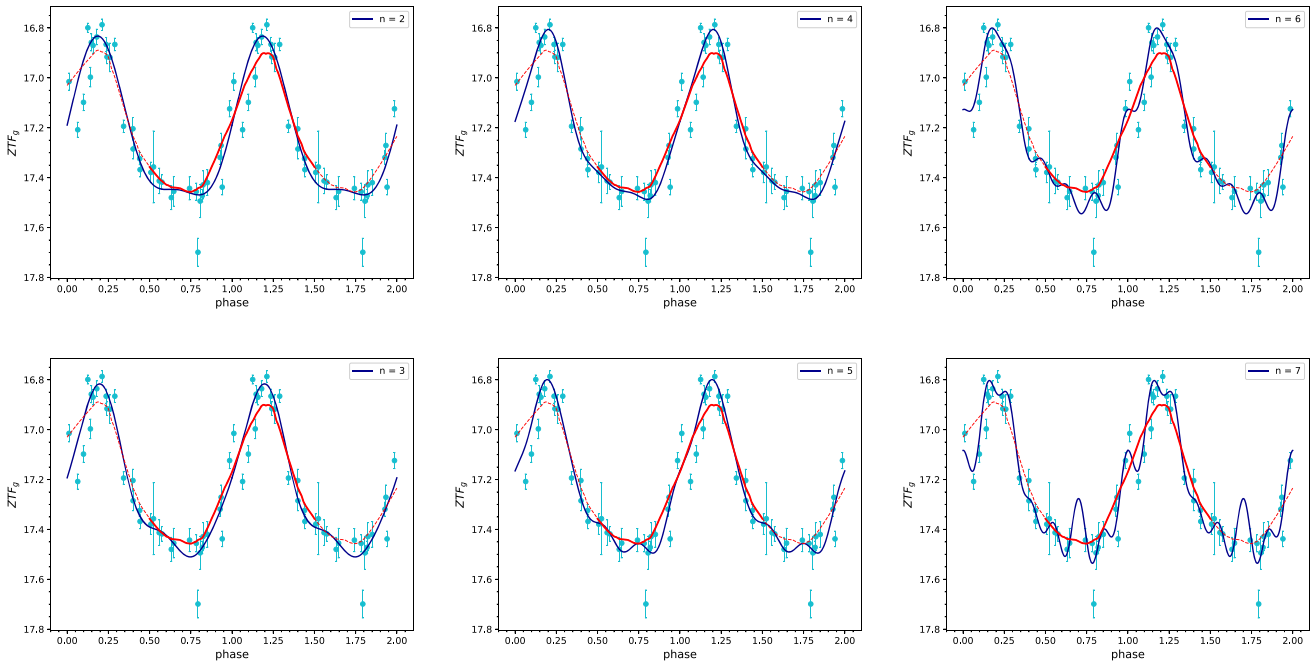

Figure 1. The ZTF g-band observed light curve data for NGC 6254 V20 fitted with various nth-order of the Fourier expansion (dark solid curves). The Baart's condition suggested the best Fourier fit is for $n = 6$. The dashed red curve is a smoothed curve derived from applying the LOWESS algorithm to the duplicated observed light curve from phase 0 to 2. The two problems mentioned in the text can be seen on the smoothed curve, such that this curve is disjointed at phase 0 and 2 (i.e., nonperiodic), and a slight deviation of the smoothed curve from the data points can be seen around phase ∼0. Therefore, we only compare the smoothed curve to the fitted Fourier expansion for different n at phases between 0.5 and 1.5 (the solid red curve). Based on such approach, the best Fourier order was found to be $n = 4$ for this observed light curve.

this light curve. The resulted smoothed curve is shown as the dashed red curve in Figure 1. We then fit the original observed light curve with various low-order (typically $n = 2$ to 5) Fourier expansions. The best Fourier order was chosen if the fitted Fourier expansion is closest to the smoothed curve within the phase of 0.5 to 1.5 (the solid red curve in Figure 1). For the example light curve shown in Figure 1, the best Fourier order was found to be $n = 4$ based on the smooth LOWESS curve. We have applied this method in our two-step period refining process mentioned earlier. The best-fit Fourier expansion was also used to obtain the intensity mean magnitude ($\langle m \rangle$, where $m = \{g, r, i\}$) and amplitude for a given light curve.

3.3. Selection of the Final Sample

Given the crowded nature of globular clusters, it is unavoidable that some of the ZTF light curves will be affected by blending. We visually inspected all of the ZTF light curves and looked for light curves that showing signs of blending, such as the light curve is flat, or the light curves exhibit too much scatter. After visual inspections, we rejected ∼60% of the SXP stars in our samples. Some of these light curves were also rejected due to reasons other than blending, including the periods found were wrong, the amplitudes unusually large, etc. ZTF light curves for few examples of the rejected SXP stars are displayed in Figure 2. Therefore, we finally selected 49 SXP stars in our sample, some examples of their ZTF light curves are shown in Figure 3. Table 1 summarized the observed properties of these selected SXP stars.

Figure 4 presents the fitted amplitudes as a function of logarithmic $P_{\rm LSM}$. As can be seen from this Figure, the visually selected SXP stars occupy a rather narrow range in $\log P_{\rm LSM}$ from ~ -1.0 to ~ -1.5. On the other hand, the rejected SXP stars spanned a wide range in $\log P_{\rm LSM}$, including some of them near the boundaries of 0.005 days ($\log P_{\rm LSM} = -2.3$) and 0.500 days ($\log P_{\rm LSM} = -0.3$) when performing the period refinement using the LSM module. These periods were incorrect suggesting the ZTF light curves on these SXP stars could be affected by blending, hence they should be excluding from the sample. The only exception is NGC 6838 P13 (marked as a green filled square in Figure 4), at which its ZTF light curves are fine but it has a much longer period than other selected SXP stars.

ZTF light curves for NGC 6838 P13, folded with $P_{\rm LSM} = 0.30585$ days found in Section 3.1, are shown in the left panel of Figure 5. This star has the longest period in the Cohen & Sarajedini (2012) catalog; however, in its discovery paper (Park & Nemec 2000) it was commented as a possible SXP star. Indeed, this star was classified as an eclipsing binary in Gaia Data Release (DR) 3 variability catalog (Eyer et al. 2022, with Gaia DR3 ID of 1821624895912072576). The Gaia DR3 eclipsing binary catalog (Mowlavi & Holl 2022) gives an orbital period of 0.61171621 days for this star, which is close to $2 \times P_{\rm LSM}$. Alternate minima can be seen from the ZTF light curves folded with $2 \times P_{\rm LSM}$, confirming the eclipsing binary nature of this star (see right panel of Figure 5) and hence it was removed from the sample.

4. The PL and PW Relations

Mean magnitudes for SXP stars listed in Table 1 were converted to absolute magnitudes by adopting the homogeneous distances (D) to their host globular clusters (Baumgardt & Vasiliev 2021), together with reddening values E returned from the `Bayerstar2019` 3D reddening map (Green et al. 2019).[10]

[10] See http://argonaut.skymaps.info/usage.

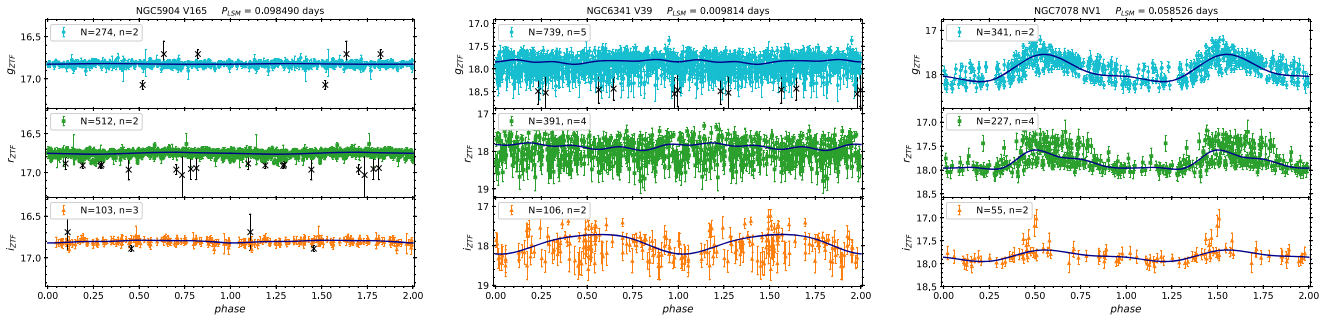

Figure 2. Examples of the light curves for rejected SXP stars in our sample. *N* represents the number of data points in the light curve. The solid curves are the fitted Fourier expansion with the best-fit Fourier order given as *n*. Black crosses are rejected data points based on the two-step period refining process as described in Section 3.1.

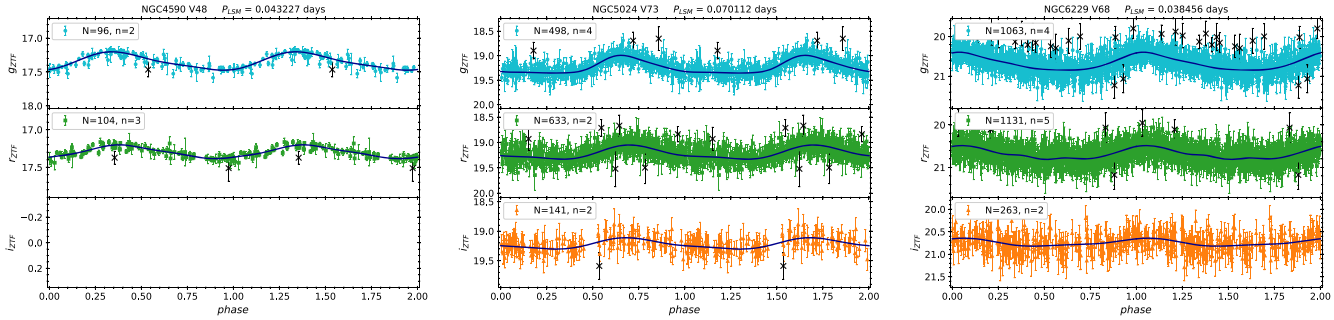

Figure 3. Same as Figure 2, but for SXP stars selected in the final sample.

4.1. Modes Identification with V-band PL Relation

Since all of the SXP stars listed in Table 1 have mean magnitudes in the *gr* band, we converted these mean magnitudes to the *V* band via the transformation provided in Tonry et al. (2012). Figure 6 presents the extinction-corrected PL relation in the *V*-band, overlaid with several *V*-band PL relation for fundamental-mode (F) pulsators taken from literature (solid lines in Figure 6). The dashed and dotted lines in Figure 6 are the PL relations for the first-overtone (1O) and second-overtone (2O) pulsators with the same PL relations as F pulsators, but shifted with a period ratio of $1O/F = 0.783$ and $2O/F = 0.571$ (see Arellano Ferro et al. 2011, and reference therein), respectively. The PL relations from Cohen & Sarajedini (2012) and Martinazzi et al. (2015b) represent the two "extremes" among the available *V*-band PL relations, and the Arellano Ferro et al. (2011) PL relation lies near the middle of them.

The six SXP stars located along the 2O PL relation from Arellano Ferro et al. (2011) are clearly pulsating in the second-overtone mode. After fundamentalized their periods, they do lie along the fundamental-mode PL relation as shown in the left panel of Figure 7. Hence, these six SXP stars are classified as 2O SXP stars. The selection of 1O SXP stars, however, are nontrivial as their locations on the PL plane could be overlapped with F SXP stars. Therefore, we first calculated the residuals from the 1O PL relation for each SXP stars (after excluding the six 2O SXP stars), and rank these residuals in ascending order. We then fundamentalized the periods one-by-one for SXP stars in this list, and fit a PL relation with the rest of SXP stars. This procedure was terminated when the dispersion of the fitted PL relation reached the minimum, and we identified 15 SXP stars pulsating in the first-overtone mode. These 1O SXP stars are marked with squares in the right panel of Figure 7. The rest of the SXP stars were then classified as fundamental-mode SXP stars. The identified pulsation modes for our final sample of SXP stars are given in Table 1.

4.2. The Multiband Relations

After fundamentalized the periods for 1O and 2O SXP stars, we first examined the period-color (PC) and period-*Q*-index (PQ) relations in the *gri*-band for these SXP stars, where $Q = (g-r) - 1.395(r-i)$ is reddening-free by construction (see Ngeow et al. 2022b, and references therein), as presented in Figure 8. NGC 6341 V33 appears to be an outlier in the PC relations, especially the $(g-i)$ PC relation. Note that this star is $\sim$1 mag brighter in *r* band than V41 in the same cluster (see Table 1), suggesting ZTF photometry for V33 could be affected by blending. Hence, we further excluded NGC 6341 V33 when fitting for various relations. For the remaining SXP stars, the fitted PC relations are:

$$(g-r) = 0.247[\pm0.064]\log P + 0.342[\pm0.081], \quad (1)$$

$$(r-i) = 0.079[\pm0.042]\log P + 0.029[\pm0.053], \quad (2)$$

$$(g-i) = 0.280[\pm0.074]\log P + 0.308[\pm0.093], \quad (3)$$

with a dispersion (σ) of 0.049, 0.029, and 0.050, respectively. Similarly, the derived PQ relation is

$$Q = 0.091[\pm0.080]\log P + 0.238[\pm0.101],\ \sigma = 0.054. \quad (4)$$

We then fit a PL relation to the transformed *V*-band mean magnitudes and obtained the following *V*-band PL relation:

$$M_V = -2.804[\pm0.035]\log P - 0.645[\pm0.044],$$
$$\sigma_V = 0.133. \quad (5)$$

Table 1
Observed Properties of the Final Selected SXP Stars in Globular Clusters

G. C.	Var. Name	$P_{\rm lit}$[a] (days)	$P_{\rm LSM}$ (days)	Mode[b]	N_g	N_r	N_i	$\langle g\rangle$	$\langle r\rangle$	$\langle i\rangle$	D[c]	E[d]
NGC 0288	V5	0.05107	0.05106683	1O	184	180	11	17.475	17.524	⋯	8.99 ± 0.09	0.016 ± 0.002
NGC 4590	V48	0.04320	0.04322702	2O	96	104	0	17.344	17.298	⋯	10.40 ± 0.10	0.000 ± 0.000
NGC 4590	V50	0.06580	0.06581527	1O	89	94	0	17.572	17.436	⋯	10.40 ± 0.10	0.000 ± 0.000
NGC 5024	V73	0.07010	0.07011209	F	498	633	141	19.228	19.212	19.218	18.50 ± 0.18	0.000 ± 0.000
NGC 5024	V74	0.04540	0.04537313	1O	874	1218	245	19.146	19.161	19.213	18.50 ± 0.18	0.000 ± 0.000
NGC 5024	V75	0.04430	0.04424759	F	823	1100	225	19.549	19.518	19.556	18.50 ± 0.18	0.000 ± 0.000
NGC 5024	V76	0.04150	0.04148953	F	718	898	187	19.777	19.840	19.914	18.50 ± 0.18	0.000 ± 0.000
NGC 5024	V77	0.07690	0.07838129	1O	931	1330	262	18.558	18.496	18.544	18.50 ± 0.18	0.000 ± 0.000
NGC 5024	V79	0.04630	0.04631969	2O	910	1298	257	18.832	18.687	18.713	18.50 ± 0.18	0.036 ± 0.002
NGC 5024	V89	0.04340	0.04547359	F	807	1091	222	19.597	19.597	19.653	18.50 ± 0.18	0.000 ± 0.000
NGC 5024	V90	0.03850	0.03849888	1O	900	1231	250	19.107	19.112	19.180	18.50 ± 0.18	0.000 ± 0.000
NGC 5024	V93	0.04010	0.04254658	2O	910	1277	256	18.777	18.733	18.802	18.50 ± 0.18	0.000 ± 0.000
NGC 5024	V96	0.03930	0.03926814	F	791	1049	220	19.540	19.479	19.545	18.50 ± 0.18	0.002 ± 0.002
NGC 5024	V100	0.04820	0.04819481	F	886	1197	243	19.319	19.256	19.332	18.50 ± 0.18	0.002 ± 0.002
NGC 5024	V101	0.05250	0.05251568	F	573	759	154	19.289	19.314	19.310	18.50 ± 0.18	0.000 ± 0.000
NGC 5053	BS28	0.04547	0.04502879	F	415	546	112	19.313	19.303	19.392	17.54 ± 0.23	0.000 ± 0.000
NGC 5053	V11	0.03700	0.03700038	1O	444	580	118	19.379	19.347	19.430	17.54 ± 0.23	0.000 ± 0.000
NGC 5053	V12	0.03765	0.03754719	F	441	565	107	19.598	19.610	19.689	17.54 ± 0.23	0.000 ± 0.000
NGC 5053	V13	0.03396	0.03416461	F	385	456	93	19.630	19.668	19.791	17.54 ± 0.23	0.000 ± 0.000
NGC 5466	V31	0.04030	0.04026386	1O	424	655	179	18.802	18.763	18.843	16.12 ± 0.16	0.000 ± 0.000
NGC 5466	V32	0.04500	0.04496170	F	363	563	152	19.252	19.278	19.401	16.12 ± 0.16	0.000 ± 0.000
NGC 5466	V33	0.04990	0.04985460	1O	415	618	159	18.846	18.803	18.916	16.12 ± 0.16	0.000 ± 0.000
NGC 5466	V34	0.05070	0.05149370	1O	444	686	185	18.714	18.679	18.755	16.12 ± 0.16	0.000 ± 0.000
NGC 5466	V35	0.05050	0.05047364	F	428	653	174	19.078	19.047	19.138	16.12 ± 0.16	0.000 ± 0.000
NGC 5466	V36	0.05520	0.05518525	1O	366	596	174	18.724	18.651	18.691	16.12 ± 0.16	0.000 ± 0.000
NGC 5466	V39	0.04800	0.04798352	F	343	338	36	19.087	19.079	19.138	16.12 ± 0.16	0.000 ± 0.000
NGC 5897	V9	0.05060	0.04816860	F	88	99	0	18.814	18.721	⋯	12.55 ± 0.24	0.096 ± 0.002
NGC 5904	V166	0.04170	0.04167214	1O	381	744	132	17.099	17.112	17.195	7.48 ± 0.06	0.004 ± 0.002
NGC 5904	V167	0.04740	0.04745436	2O	400	769	135	17.009	16.970	17.026	7.48 ± 0.06	0.074 ± 0.002
NGC 6171	V26	0.05260	0.05551172	F	116	169	0	18.090	17.625	⋯	5.63 ± 0.08	0.430 ± 0.000
NGC 6205	V47	0.06526	0.06525557	F	1255	1137	192	17.224	17.129	17.193	7.42 ± 0.08	0.000 ± 0.000
NGC 6205	V50	0.06175	0.06175429	F	1290	1308	254	17.052	16.969	16.993	7.42 ± 0.08	0.000 ± 0.000
NGC 6218	V25	0.04903	0.04903408	F	191	335	4	17.176	16.988	⋯	5.11 ± 0.05	0.194 ± 0.006
NGC 6229	V68	0.03850	0.03845637	F	1063	1131	263	20.657	20.675	20.744	30.11 ± 0.47	0.004 ± 0.002
NGC 6254	V17	0.03695	0.05564910	F	52	108	1	17.601	17.331	⋯	5.07 ± 0.06	0.272 ± 0.002
NGC 6254	V20	0.05060	0.05060309	F	35	82	1	17.213	17.008	⋯	5.07 ± 0.06	0.226 ± 0.007
NGC 6341	V33	0.07509	0.07509381	2O	1486	1407	420	16.455	16.169	16.045	8.50 ± 0.07	0.000 ± 0.000
NGC 6341	V41	0.05595	0.05594717	1O	1633	1597	454	17.147	17.132	17.214	8.50 ± 0.07	0.000 ± 0.000
NGC 6402	V177	0.06898	0.06898326	F	188	549	1	19.469	18.782	⋯	9.14 ± 0.25	0.560 ± 0.003
NGC 6656	KT-04	0.03600	0.03707136	1O	100	601	0	16.948	16.629	⋯	3.30 ± 0.04	0.374 ± 0.002
NGC 6656	KT-28	0.05500	0.05888543	1O	88	552	0	16.447	16.033	⋯	3.30 ± 0.04	0.338 ± 0.002
NGC 6779	V15	0.04552	0.04545172	1O	363	656	24	18.752	18.421	⋯	10.43 ± 0.14	0.180 ± 0.000
NGC 6934	V52	0.06356	0.06356308	F	258	562	117	19.033	18.870	18.889	15.72 ± 0.17	0.080 ± 0.003
NGC 6934	V92	0.04586	0.04384961	F	199	463	92	19.607	19.442	19.494	15.72 ± 0.17	0.102 ± 0.002
NGC 6981	V55	0.04700	0.04703276	F	196	228	0	19.649	19.609	⋯	16.66 ± 0.18	0.038 ± 0.002
NGC 7078	V156	0.04060	0.04062126	F	701	805	181	18.491	18.487	18.539	10.71 ± 0.10	0.052 ± 0.005
NGC 7099	V20	0.04020	0.04019862	F	165	168	0	17.784	17.747	⋯	8.46 ± 0.09	0.000 ± 0.000
NGC 7492	V6	0.05660	0.05359233	2O	176	203	43	19.157	19.034	19.068	24.39 ± 0.57	0.038 ± 0.002

Notes.
[a] Published period as given in the literature.
[b] Pulsation mode based on the V-band PL relation, see Section 4.1 for more details.
[c] Distance of the host globular clusters in kpc, adopted from Baumgardt & Vasiliev (2021).
[d] Reddening value returned from the `Bayerstar2019` 3D reddening map (Green et al. 2019) at the location of the SXP stars in the globular clusters. Extinction corrections on each filters are: $A_g = 3.518E$, $A_r = 2.617E$ and $A_i = 1.971E$ (Green et al. 2019).

The fitted fundamental-mode V-band PL relation, shown in Figure 9, is similar to the theoretical V-band PL relation presented in Fiorentino et al. (2015; $-2.847\log P - 0.45$ at $Z = 0.0001$). Since there is no clear trend of the metallicity on the V-band PL relation, as displayed in Figure 9, as well as a rather small sample size with 47 SXP stars, we do not include a metallicity term when fitting the PL relation.

In a similar manner, we derived the following *gri*-band PL relations:

$$M_g = -2.719[\pm0.031]\log P - 0.529[\pm0.039],$$
$$\sigma_g = 0.135, \quad (6)$$
$$M_r = -2.907[\pm0.031]\log P - 0.792[\pm0.039],$$
$$\sigma_r = 0.135, \quad (7)$$

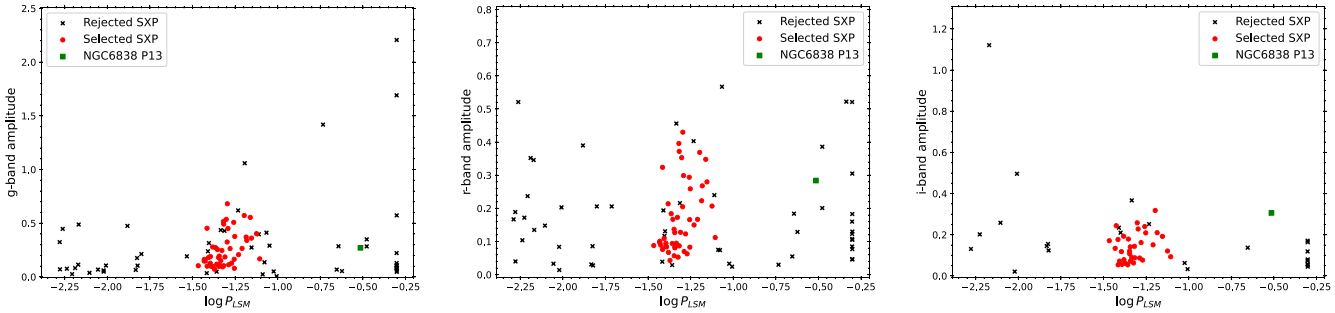

Figure 4. Amplitudes as a function of $\log P_{\rm LSM}$ for the SXP stars in the sample. See text for further discussion on NGC 6838 P13.

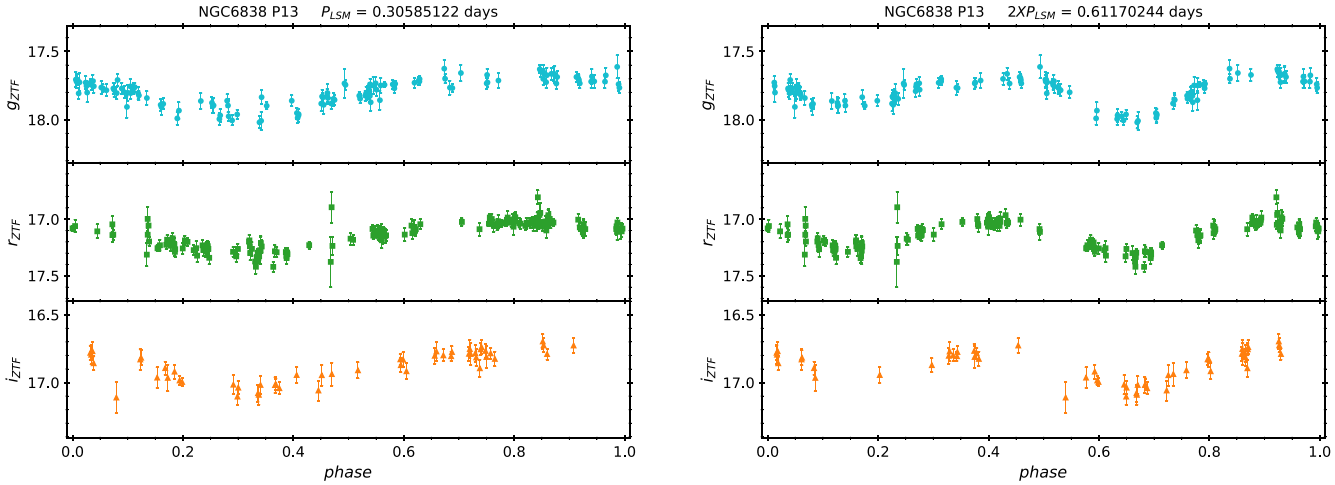

Figure 5. ZTF light curves for NGC 6838 P 13 folded with $P_{\rm LSM}$ (left panel) and twice of $P_{\rm LSM}$ (right panel).

$$M_i = -2.917[\pm0.035]\log P - 0.737[\pm0.043],$$
$$\sigma_i = 0.129. \quad (8)$$

For the PW relations, following our previous work (see Ngeow et al. 2022b, and reference therein), we obtained the three PW relations as given below:

$$W_g^{gr} = -3.458[\pm0.031]\log P - 1.561[\pm0.038], \quad (9)$$
$$W_r^{ri} = -3.092[\pm0.034]\log P - 0.743[\pm0.043], \quad (10)$$
$$W_g^{gi} = -3.195[\pm0.034]\log P - 1.024[\pm0.043]. \quad (11)$$

Dispersions of these PW relations, however, are larger than the PL relations, with $\sigma = 0.216$, 0.163, and 0.161, respectively. These *gri*-band PL and PW relations are presented in Figure 10.

5. Example of Application: the Only SXP Star in Crater II

Vivas et al. (2020) reported the detection of one SXP star, with an ID of V97, in dwarf galaxy Crater II using *gi*-band time-series DECam observations. This SXP star has a rather long pulsation period, $P = 0.23461$ days, much longer than the SXP stars listed in Table 1. Assuming V97 is pulsating in fundamental-mode, then the predicted absolute magnitudes at this period, based on Equations (6) and (8), are $M_g(V97) = 1.18 \pm 0.18$ mag and $M_i(V97) = 0.79 \pm 0.19$ mag, respectively. Since the photometry presented in Vivas et al. (2020) were calibrated to the SDSS photometric system, we transformed the mean *gi*-band magnitudes for V97, after correcting for extinction using the `Bayerstar2019` 3D reddening map (Green et al. 2019), to the PAN-STARRS1 system based on the transformations given in Tonry et al. (2012). These transformations, however, required the $(g-r)$

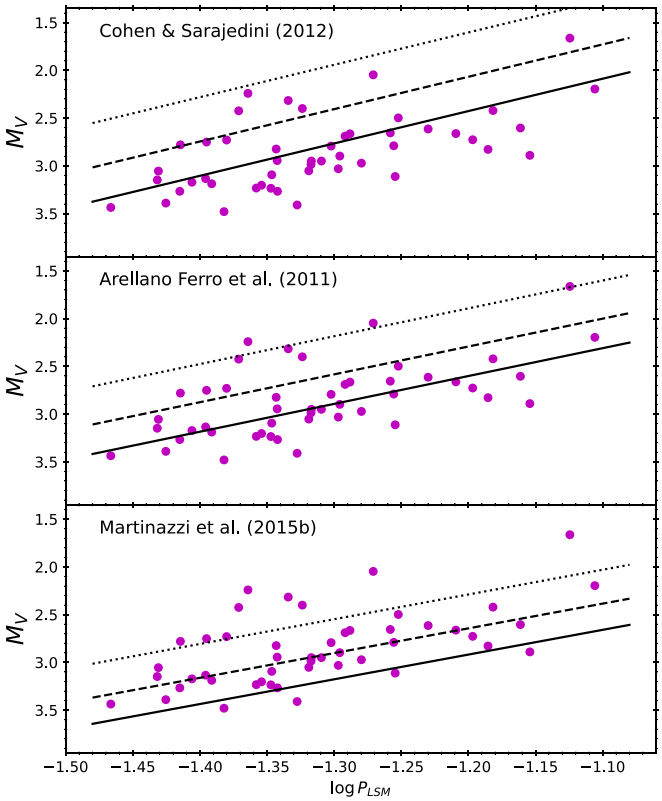

Figure 6. Comparison of the observed *V*-band PL relations for the 48 SXP stars listed in Table 1 to the published PL relations for fundamental-mode pulsators (solid lines) in the literature. The dashed and dotted lines are the corresponding PL relations for the first-overtone and the second-overtone pulsators, respectively (see text for more details).

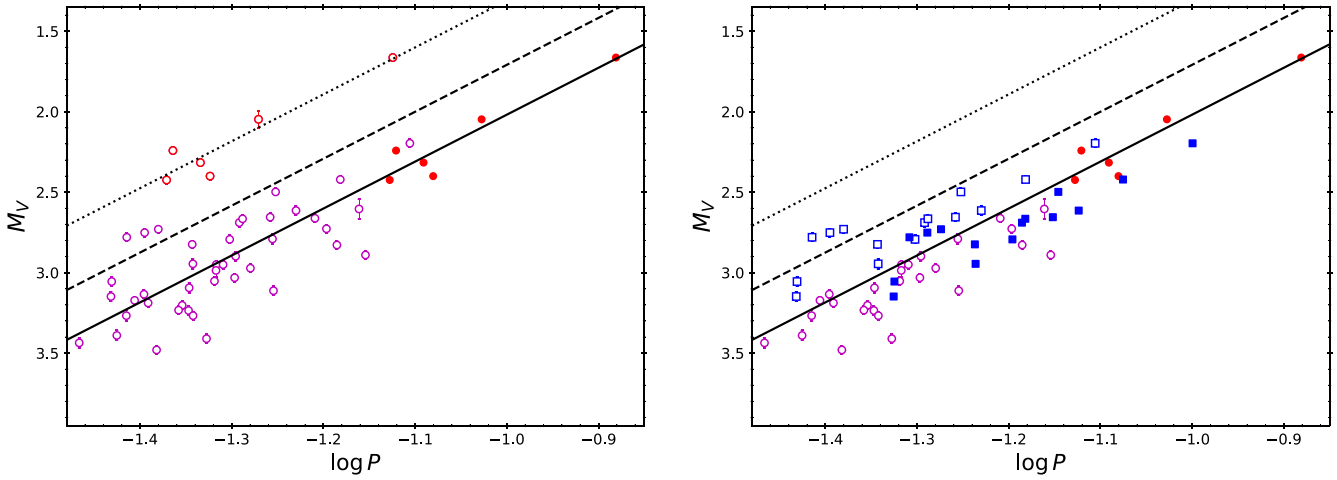

Figure 7. Left panel: the transformed V-band mean magnitudes for the 48 SXP stars, shown as open circles, listed in Table 1 as a function of pulsation period P. The solid, dashed, and dotted lines are the F, 1O, and 2O PL relation published in Arellano Ferro et al. (2011; see text for more details). SXP stars labeled as open red circles are assumed to pulsate in the second-overtone mode. After fundamentalizing their periods, their new locations on the PL plane are marked as filled red circles. Right panel: same as the left panel, but for the 15 SXP stars identified as pulsating in the first-overtone mode, as described in the text. Open and filled blue squares are their locations on the PL plane before and after fundamentalizing their periods, respectively.

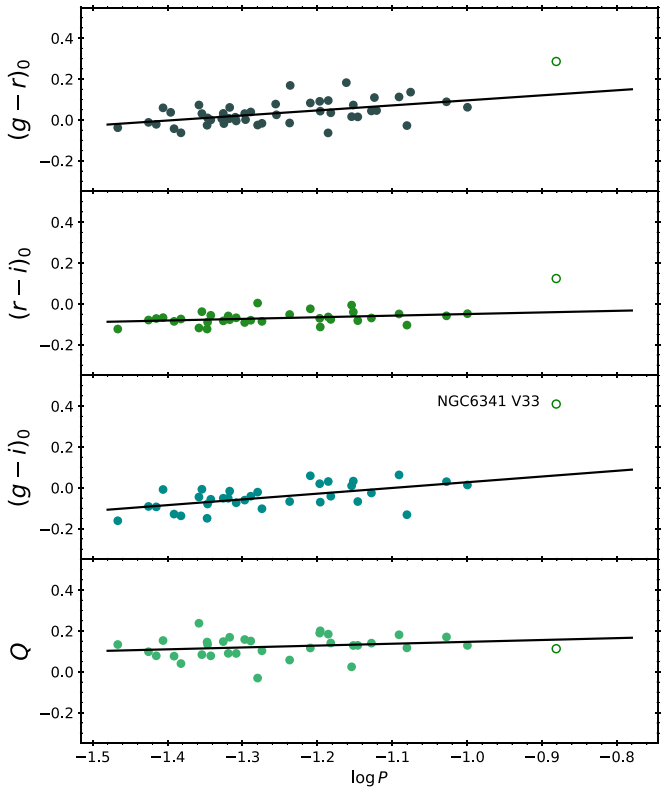

Figure 8. Extinction-corrected PC relations and the extinction-free PQ relations in the *gri* band. Note that the periods for 1O and 2O SXP have been fundamentalized. The open circle marks the outlier NGC 6341 V33 in the $(g-i)$ PC relation.

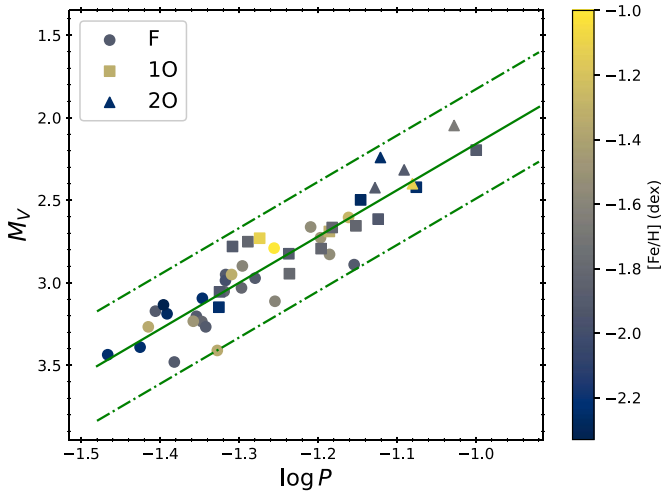

Figure 9. Fitted V-band PL relation, shown as the solid line, to the F (circles), 1O (squares), and 2O (triangles) SXP stars in the sample. The dotted-dashed lines represent the $\pm 2.5\sigma$ boundaries, where σ is the dispersion of the fitted PL relation. The data points are color coded with the metallicities of the host globular clusters ([Fe/H]), adopted from the GlObular clusTer Homogeneous Abundances Measurements survey (Dias et al. 2015, 2016a, 2016b; Vásquez et al. 2018), where the metallicity ranged from -1.00 dex (NGC 6171) to -2.33 dex (NGC 7099).

color for the target star, which is absent from Vivas et al. (2020) observations. Hence, we estimated the $(g-r)$ color using Equation (1), which gives a predicted color of 0.19 ± 0.06 mag for V97. The resulted gi-band distance moduli are $\mu_g = 20.02 \pm 0.18$ mag and $\mu_i = 20.02 \pm 0.18$ mag, respectively. Similarly, the predicted absolute W_g^{gi} Wesenheit magnitude is $M_W(V97) = 0.99 \pm 0.22$ mag, which give a (extinction-free) distance modulus of $\mu_W = 20.03 \pm 0.23$ mag.

Clearly, these distance moduli are smaller than $\mu \sim 20.33$ mag found by Vivas et al. (2020) based on RR Lyrae. Vivas et al. (2020) suspected that V97 could be pulsating in the first-overtone mode. If we fundamentalized the period of V97 and repeated the above calculations, the resulted distance moduli became $\mu_g = 20.31 \pm 0.19$ mag, $\mu_i = 20.33 \pm 0.19$ mag, and $\mu_W = 20.37 \pm 0.24$ mag. These distance moduli are consistent with the values found by Vivas et al. (2020) and Ngeow et al. (2022a), supporting the assumption that V97 is indeed pulsating in the first-overtone mode.

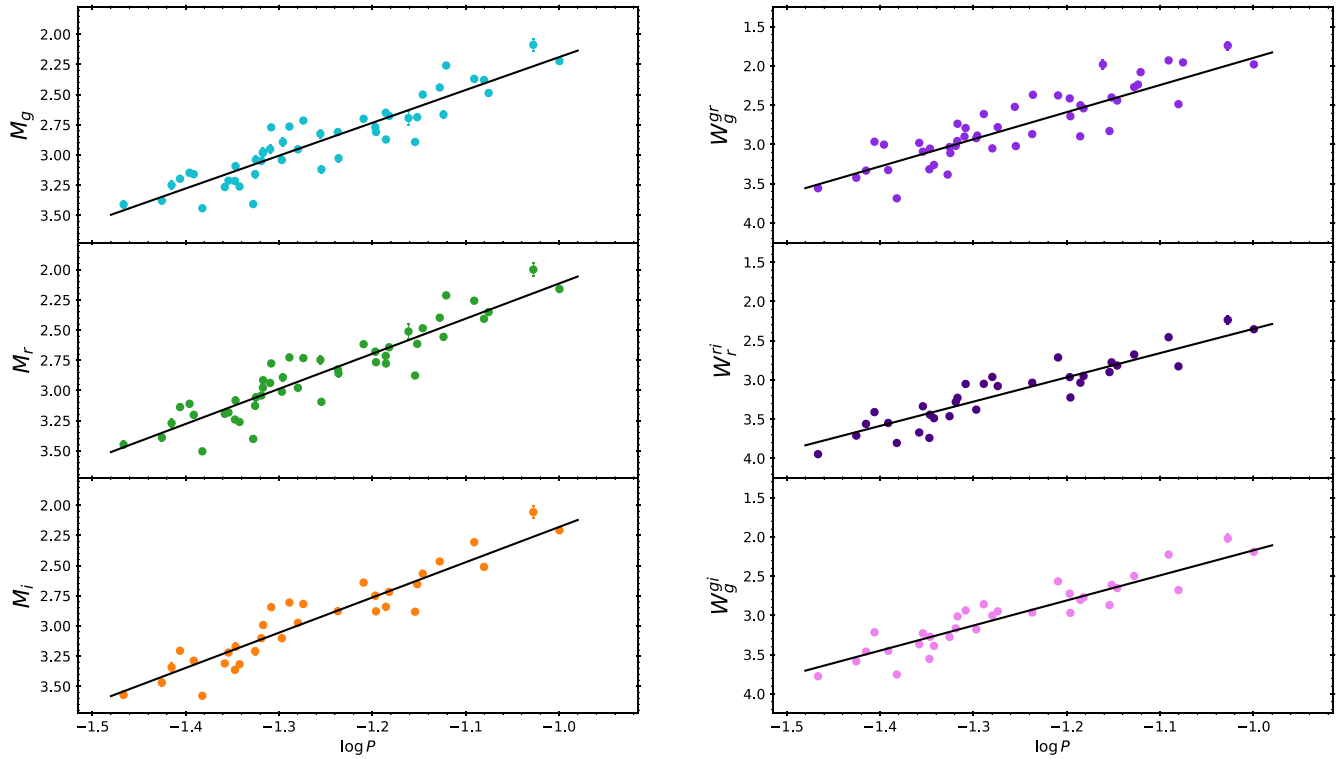

Figure 10. Extinction-corrected PL relations (left panel) and the extinction-free PW relations (right panel) in the *gri* band for our sample of SXP stars in the globular clusters. The solid lines are the fitted relations as given in Equations (6) to (11).

6. Conclusions

Based on homogeneous distances to globular clusters, we calibrated the PL and PW relations for SXP stars in the *gri* band using the light curve data obtained from ZTF. In addition, we have also updated the *V*-band PL relation after transforming the *gr*-band mean magnitudes to the *V* band for our sample of SXP stars, as well as deriving the *gri*-band PC relations and PQ relation for the first time. We tested our derived relations on the only SXP star discovered in dwarf galaxy Crater II. Assuming this SXP star is pulsating in first-overtone mode, the derived distance moduli to Crater II using our PL and PW relations are consistent with value given in the literature.

In the coming years when LSST is in its routine operations, it is expected to detect more SXP variables in Crater II. According to our derived PL relations and adopting the distance modulus of Crater II to be ∼20.33 mag, the shortest period for SXP stars at $\log P \sim -1.5$ (or ∼0.032 days) would have a mean magnitude of ∼23.9 mag in the *g* band, which is brighter than the detection limit of 25.0 mag from a single epoch LSST observations (Ivezić et al. 2019). Hence, it is possible that LSST could detect additional SXP stars in Crater II, as well as finding new SXP stars in other dwarf galaxies with similar distances to Crater II. Our empirical *gri*-band PL and PW relations for SXP variables will improve the distance determination using these Population II short-period pulsating stars, and provide an independent cross-check to other distance indicators such as RR Lyrae and Type II Cepheids.

We thank the useful discussions and comments from an anonymous referee that improved the manuscript. We are thankful for funding from the National Science and Technology Council (Taiwan) under the contracts 107-2119-M-008-014-MY2, 107-2119-M-008-012, 108-2628-M-007-005-RSP, and 109-2112-M-008-014-MY3.

Based on observations obtained with the Samuel Oschin Telescope 48 inch Telescope at the Palomar Observatory as part of the Zwicky Transient Facility project. Z.T.F. is supported by the National Science Foundation under grants No. AST-1440341 and AST-2034437, and a collaboration including current partners Caltech, IPAC, the Weizmann Institute of Science, the Oskar Klein Center at Stockholm University, the University of Maryland, Deutsches Elektronen-Synchrotron and Humboldt University, the TANGO Consortium of Taiwan, the University of Wisconsin at Milwaukee, Trinity College Dublin, Lawrence Livermore National Laboratories, IN2P3, University of Warwick, Ruhr University Bochum, Northwestern University and former partners the University of Washington, Los Alamos National Laboratories, and Lawrence Berkeley National Laboratories. Operations are conducted by COO, IPAC, and UW.

This research has made use of the SIMBAD database and the VizieR catalog access tool, operated at CDS, Strasbourg, France. This research made use of Astropy,[11] a community-developed core Python package for Astronomy (Astropy Collaboration et al. 2013, 2018, 2022).

Facility: PO:1.2 m.

Software: `astropy` (Astropy Collaboration et al. 2013, 2018, 2022), `dustmaps` (Green 2018), `gatspy` (VanderPlas & Ivezić 2015), `Matplotlib` (Hunter 2007), `NumPy` (Harris et al. 2020), `SciPy` (Virtanen et al. 2020), `statsmodels` (Seabold & Perktold 2010).

[11] http://www.astropy.org

ORCID iDs

Chow-Choong Ngeow https://orcid.org/0000-0001-8771-7554
Anupam Bhardwaj https://orcid.org/0000-0001-6147-3360
Matthew J. Graham https://orcid.org/0000-0002-3168-0139
Brian F. Healy https://orcid.org/0000-0002-7718-7884
Russ R. Laher https://orcid.org/0000-0003-2451-5482
Reed Riddle https://orcid.org/0000-0002-0387-370X
Avery Wold https://orcid.org/0000-0002-9998-6732

References

Ahumada, J. A., Arellano Ferro, A., Bustos Fierro, I. H., et al. 2021, NewA, 88, 101607
Arellano Ferro, A., Figuera Jaimes, R., Giridhar, S., et al. 2011, MNRAS, 416, 2265
Arellano Ferro, A., Giridhar, S., & Bramich, D. M. 2010, MNRAS, 402, 226
Arellano Ferro, A., Mancera Piña, P. E., Bramich, D. M., et al. 2015, MNRAS, 452, 727
Arellano Ferro, A., Yepez, M. A., Muneer, S., et al. 2020, MNRAS, 499, 4026
Astropy Collaboration, Price-Whelan, A. M., & Lim, P. L. 2022, ApJ, 935, 167
Astropy Collaboration, Price-Whelan, A. M., Sipőcz, B. M., et al. 2018, AJ, 156, 123
Astropy Collaboration, Robitaille, T. P., Tollerud, E. J., et al. 2013, A&A, 558, A33
Barac, N., Bedding, T. R., Murphy, S. J., & Hey, D. R. 2022, MNRAS, 516, 2080
Baumgardt, H., & Vasiliev, E. 2021, MNRAS, 505, 5957
Bellm, E., & Kulkarni, S. 2017, NatAs, 1, 0071
Bellm, E. C., Kulkarni, S. R., Graham, M. J., et al. 2019, PASP, 131, 018002
Bhardwaj, A., Kanbur, S. M., Singh, H. P., et al. 2015, MNRAS, 447, 3342
Bramich, D. M., Arellano Ferro, A., Jaimes, R. F., et al. 2012, MNRAS, 424, 2722
Chambers, K. C., Magnier, E. A., Metcalfe, N., et al. 2016, arXiv:1612.05560
Clement, C. M. 2017, yCat, V/150
Clement, C. M., Muzzin, A., Dufton, Q., et al. 2001, AJ, 122, 2587
Cleveland, W. S. 1979, Journal of the American Statistical Association, 74, 829
Cohen, R. E., & Sarajedini, A. 2012, MNRAS, 419, 342
Deb, S., & Singh, H. P. 2009, A&A, 507, 1729
Dekany, R., Smith, R. M., Riddle, R., et al. 2020, PASP, 132, 038001
Deras, D., Arellano Ferro, A., Bustos Fierro, I., et al. 2022, RMxAA, 58, 121
Deras, D., Arellano Ferro, A., Lázaro, C., et al. 2019, MNRAS, 486, 2791
Dias, B., Barbuy, B., Saviane, I., et al. 2015, A&A, 573, A13
Dias, B., Barbuy, B., Saviane, I., et al. 2016a, A&A, 590, A9
Dias, B., Saviane, I., Barbuy, B., et al. 2016b, Msngr, 165, 19
Eyer, L., Audard, M., Holl, B., et al. 2022, arXiv:2206.06416
Figuera Jaimes, R., Arellano Ferro, A., Bramich, D. M., et al. 2013, A&A, 556, A20
Fiorentino, G., Lanzoni, B., Dalessandro, E., et al. 2014, ApJ, 783, 34
Fiorentino, G., Marconi, M., Bono, G., et al. 2015, ApJ, 810, 15
Flaugher, B., Diehl, H. T., Honscheid, K., et al. 2015, AJ, 150, 150
Gaia Collaboration, De Ridder, J., Ripepi, V., et al. 2022, arXiv:2206.06075
Graham, M. J., Kulkarni, S. R., Bellm, E. C., et al. 2019, PASP, 131, 078001
Green, G. M. 2018, JOSS, 3, 695
Green, G. M., Schlafly, E., Zucker, C., et al. 2019, ApJ, 887, 93
Harris, C. R., Millman, K. J., van der Walt, S. J., et al. 2020, Natur, 585, 357
Hunter, J. D. 2007, CSE, 9, 90
Jeon, Y.-B., Kim, S.-L., Lee, M. G., et al. 2006, ApJL, 636, L129
Jeon, Y.-B., Lee, M. G., Kim, S.-L., et al. 2003, AJ, 125, 3165
Jeon, Y.-B., Lee, M. G., Kim, S.-L., et al. 2004, AJ, 128, 287
Ivezić, Z. ˇ, Kahn, S. M., Tyson, J. A., et al. 2019, ApJ, 873, 111
Kaluzny, J., Thompson, I. B., Narloch, W., et al. 2015, AcA, 65, 267
Kopacki, G. 2015, AcA, 65, 81
Kunder, A., Stetson, P. B., Catelan, M., et al. 2013, AJ, 145, 33
Lata, S., Pandey, A. K., Pandey, J. C., et al. 2019, AJ, 158, 51
Lee, D.-J., Koo, J.-R., Hong, K., et al. 2016, JKAS, 49, 295
Magnier, E. A., Sweeney, W. E., Chambers, K. C., et al. 2020, ApJS, 251, 5
Martinazzi, E., Kepler, S. O., Costa, J. E. S., et al. 2015a, MNRAS, 447, 2235
Martinazzi, E., Kepler, S. O., Costa, J. E. S., et al. 2015b, MNRAS, 449, 3535
Martínez-Vázquez, C. E., Salinas, R., Vivas, A. K., et al. 2022, ApJL, 940, L25
Masci, F. J., Laher, R. R., Rusholme, B., et al. 2019, PASP, 131, 018003
McCormac, J., Skillen, I., Pollacco, D., et al. 2014, MNRAS, 438, 3383
McNamara, D. 1997, PASP, 109, 1221
McNamara, D. H. 1995, AJ, 109, 1751
McNamara, D. H. 2011, AJ, 142, 110
Mowlavi, N., Holl, B., Lecœur-Taïbi, I., et al. 2022, arXiv:2211.00929
Navarrete, C., Catelan, M., Contreras Ramos, R., et al. 2017, A&A, 604, A120
Nemec, J., & Mateo, M. 1990, in Proc. of the Conf. 11, Confrontation Between Stellar Pulsation and Evolution, ed. C. Cacciari & G. Clementini (San Francisco CA: ASP), 64
Nemec, J. M., Nemec, A. F. L., & Lutz, T. E. 1994, AJ, 108, 222
Ngeow, C.-C., Bhardwaj, A., Dekany, R., et al. 2022a, AJ, 163, 239
Ngeow, C.-C., Bhardwaj, A., Henderson, J.-Y., et al. 2022b, AJ, 164, 154
Park, N.-K., & Nemec, J. M. 2000, AJ, 119, 1803
Petersen, J. O. 1986, A&A, 170, 59
Poretti, E., Clementini, G., Held, E. V., et al. 2008, ApJ, 685, 947
Pych, W., Kaluzny, J., Krzeminski, W., et al. 2001, A&A, 367, 148
Rodríguez, E., & López-González, M. J. 2000, A&A, 359, 597
Rozyczka, M., Narloch, W., Schwarzenberg-Czerny, A., et al. 2018, Acta Astronomica, 68, 237
Rozyczka, M., Thompson, I. B., Pych, W., et al. 2017, Acta Astronomica, 67, 203
Salinas, R., Contreras Ramos, R., Strader, J., et al. 2016, AJ, 152, 55
Santolamazza, P., Marconi, M., Bono, G., et al. 2001, ApJ, 554, 1124
Sariya, D. P., Jiang, I.-G., & Yadav, R. K. S. 2018, RAA, 18, 126
Sariya, D. P., & Yadav, R. K. S. 2015, A&A, 584, A59
Seabold, S., & Perktold, J. 2010, in Proc. of the IX Python in Science Conf., ed. S. van der Walt & J. Millman (Austin, TX: SciPy) https://conference.scipy.org/proceedings/scipy2010/pdfs/proceedings.pdf 92
Templeton, M., Basu, S., & Demarque, P. 2002, ApJ, 576, 963
Tonry, J. L., Stubbs, C. W., Lykke, K. R., et al. 2012, ApJ, 750, 99
VanderPlas, J. T., & Ivezić, Ž. 2015, ApJ, 812, 18
Vásquez, S., Saviane, I., Held, E. V., et al. 2018, A&A, 619, A13
Virtanen, P., Gommers, R., Oliphant, T. E., et al. 2020, NatMe, 17, 261
Vivas, A. K., Alonso-García, J., Mateo, M., et al. 2019, AJ, 157, 35
Vivas, A. K., & Mateo, M. 2013, AJ, 146, 141
Vivas, A. K., Walker, A. R., Martínez-Vázquez, C. E., et al. 2020, MNRAS, 492, 1061
Yepez, M. A., Arellano Ferro, A., & Deras, D. 2020, MNRAS, 494, 3212
Yepez, M. A., Arellano Ferro, A., Deras, D., et al. 2022, MNRAS, 511, 1285
Yepez, M. A., Arellano Ferro, A., Muneer, S., et al. 2018, RMxAA, 54, 15